ORIGINAL RESEARCH

Vulnerability assessment of RC buildings to lateral spreading

Fausto Somma[1] · Maxim Millen[2] · Emilio Bilotta[3] · Alessandro Flora[3] ·
Antonio Viana Da Fonseca[4]

Abstract

Large magnitude earthquakes have historically caused devastating damage to engineered structures as a result of permanent ground deformations induced by soil liquefaction (e.g. 1964 Niigata earthquake, 1995 Kobe earthquake, 2010–2011 Christchurch earthquakes). A relevant amount of such damages is directly connected to liquefaction induced lateral spreading. This paper deals with the capacity of concrete framed structures with shallow foundations to handle lateral spreading demands. A simplified force–displacement compatible model was developed to capture the loads on the shallow foundations and estimate the performance of the building. The key parameters of foundation embedment, foundation width and shear length of the pillar, as well as soil friction angle were identified as having a strong influence on the expected performance. The developed model was used to develop probabilistic fragility curves for a class of buildings representing two to five storeys reinforced concrete buildings. Field measurements from existing literature of the liquefaction induced lateral displacement demand from the the September 4, 2010 (Mw 7.1) and the February 22, 2011 (Mw 6.2) Canterbury (New Zealand) earthquakes along the Avon River were probabilistically quantified in relation to the distance from the river. Finally, the displacement demand and fragility curves were used to estimate the probability of exceeding the considered limit states as a function of the distance from the river.

Keywords Lateral spreading · Soil-structure interaction · Numerical analysis · Fragility curves · Vulnerability assessment

1 Introduction

The accumulation of permanent lateral ground displacements during earthquakes, driven by static shear stresses, is often referred to as lateral spreading. This phenomenon has been observed after several seismic events: among them, in the past three decades, those of Loma Prieta in 1989 (Boulanger et al. 1997; Holzer 1998), Hyogo-ken Nanbu (Kobe) in 1995 (Comartin et al. 1995; Hamada and Wakamatsu 1998), Kocaeli (Izmit) in 1999 (Bardet et al. 2000; Cetin et al. 2004) and Christchurch in 2010 and 2011.

✉ Fausto Somma
    fausto.somma@unina.it

Extended author information available on the last page of the article

More specifically, using the definition from Cubrinovski et al (2012), lateral spreading is the horizontal or sub-horizontal movement of a sloping or level ground close to waterways/ open face (e.g. river banks, streams and in the backfills behind quay walls) occurring at a site underlain by liquefying soil. The reduced strength of the liquefied soil combined with the inertial forces of the earthquake overcome the static equilibrium and result in lateral deformation towards the free-face or sloping ground. It is both a static and dynamic failure and hence the reason eye witnesses have seen spreading damage occur during and after an earthquake. The liquefied underlying soils are weakened and create a 'sliding mechanism' for the crust layer above which leads to very pronounced lateral displacements. Lateral spreads typically result in rigid movement of the shallow ground in block-like units as a result of extension in the direction of spreading. Hence cracks or fissures between these blocks are created, propagating in a direction perpendicular to the spreading movement (Rauch and Martin 2000). Ground cracks are typically a manifestation of lateral stretching and they occur when a block moves on average a lower horizontal displacement than the adjacent block (Robinson 2016).

Case studies from Canterbury earthquake sequence 2010–2011 from Cubrinovski et al. (2012) report major damage to buildings from differential lateral spreading, where buildings were stretched due to cracks opening under the building. This type of deformation can be particularly disastrous to buildings as the ground floor columns can experience large deformations and eventually fail. Early efforts to capture this type of loading on a building were for ground distortions related to mine excavations (e.g. Boscardin and Cording 1989), these early studies focused on both settlement and lateral extension and typically assumed that foundation distortion was equal to the ground distortion. However, Boscardin and Cording (1989) highlight and demonstrated through field case studies that foundation reinforcing, the soil-foundation interface, foundation embedment, presence of grade beams and the type of structure can all influence the expected foundation distortions. More recent vulnerability assessment models for buildings experiencing loads from landslides (Negulescu and Foerster 2010) and liquefaction induced deformation (Fotopoulou et al. 2018) have directly imposed the expected ground deformations as deformations to the foundation. While directly imposing displacements can be considered conservative, in many cases this assumption can lead to a significant overestimation of damage to buildings (Gomez-Martinez et al. 2019).

The estimation of the extent of liquefaction-induced lateral displacements is a key aspect in evaluating the performance of the building. Results from aerial photogrammetry analyses of areas struck by the 1964 and 1983 Japan earthquakes (Niigata 1964 Mw 7.5, Nihonkai-Chubu 1983 Mw 7.7) provided by Hamada et al. (1987) allowed to demonstrate that lateral spreading can occur with slopes as little as 0.3%, with a movement typically perpendicular to ground cracking and to waterways. The magnitude of displacements depended on the ground and base slope and on the thickness of the liquefied layer, and it decreased with distance from the river or the down-slope. In the presence of driving stresses or unconstrained boundaries (such as free-face near river banks), calculations show that the liquefied soil can undergo permanent lateral ground deformations as large as several meters in some cases (Cubrinovski et al. 2018).

There are several existing empirical and semi-empirical methods for estimating lique-faction-induced lateral displacements (e.g. Hamada et al. 1987; Youd and Perkins 1987; Shamoto et al. 1998a, b; Rauch and Martin 2000; Zhang et al. 2004; Faris et al. 2006; Kramer et al. 2007) based on the large collection of evidence (e.g. Bartlett and Youd 1992; Youd et al. 2002a, b). These methods have highlighted the relevant geometrical, mechanical and seismic parameters (e.g. seismic intensity, soil grain size, liquefaction resistance,

surface slope angle, height of, and distance to free face), however, they are generally accepted to be accurate only within a factor of 2 or 3 at most, and their predictive capacity tends to be worst for small-to-moderate (0.3–0.75 m) deformations (Bird et al. 2006).

This paper develops a simple, force and displacement compatible approach to modelling the loads imposed by lateral displacements on shallow foundations to remove the bias of the direct displacement approach. The approach is applied to typical low-code reinforced concrete (RC) buildings with shallow foundations to explore the extent of over conservativism in direct displacement models and understand the key parameters involved in building performance. The model is then applied as a case study to the demands experienced along the Avon River during the Canterbury earthquake sequence 2010–2011. The differential displacement demands are based on statistical quantification of field measurements from Robinson (2016) and compared to existing empirical methods. Finally the performance is quantified in terms of probability in framework of regional based vulnerability assessment of buildings against liquefaction-induced lateral spreading.

2 Soil-structure interaction model

2.1 The displacement-based approach

The primary damage to buildings during earthquakes is shaking damage, therefore the modification to the ground shaking due to liquefaction is extremely important in the context of quantifying building performance. The current understanding is that liquefaction causes a reduction in soil shear stiffness (and resistance), increase in soil shear strain, and can amplify and reduce particular frequencies of the surface shaking. Therefore, the amplification or reduction of the surface shaking, in terms of peak values, due to liquefaction is function of the frequency content of the outcrop motion and of the geotechnical specificities of the site.The reduced stiffness lengthens the characteristic site period and means that shear waves dissipate more energy over the same distance because shear wave speeds have reduced (and consequently the wavelength), this is particularly evident for small cycle (high frequency) waves. The energy dissipation per cycle is also increased because the softer soil undergoes larger nonlinear strains and therefore the liquefied layer can act as a high-pass filter.

In the specific case of the Lateral Spreading where a non-liquefiable crust lies on a liquefiable layer, Bouckovalas et al. (2016) investigated the amplification of the shaking response of a two-layered visco-elastic soil deposit resting on a rigid bedrock. The top layer represented a non-liquefied crust and the lower layer represented a liquefied deposit, with a soil shear wave velocity ratio between the two layers (Vs,L/Vs,c) of 0.15, the densities were equal, the liquefied layer was three times thicker than the crust (HL/HC), and the viscous damping of the crust and lower deposit set to 10% and 15% respectively. This simple analytical model indicated that amplification of the excitation frequency would occur when the ratio of the height of the liquefied layer to the excitation wave length in the liquefied layer (HL/λ*L) was less than 0.25, while de-amplification would occur above this ratio. The properties where then varied and the simple model indicated that changing the ratio of densities, the ratio of shear wave velocities and changing the crust damping all had negligible effect on the transfer function. Increasing the liquefied layer damping reduced the amplitude of amplification and changing the ratio of crust thickness to liquefied layer

thickness caused a major change in the relationship. Further discussion on this is beyond the scope of this paper.

There are a number of deformation modes that buildings may experience when subjected to liquefaction-induced ground deformations (Bird et al. 2006). With reference to vertical settlements, these modes can be divided into two broad categories: rigid-body movements, whereby the structure moves without significant internal deformations, possibly attaining a geotechnical limit state, and differential movements among structural elements, that induce stress increments into the structure and may thus lead to structural limit states (Marino 1997). The type of response depends primarily on the relative stiffness of the superstructure and foundation with respect to the soil stiffness and heterogeneity of the ground conditions allowing differential movements to occur. For shallow foundations, which are those of interest in this paper, the distinction will depend on whether these are continuous and rigid (e.g. thick rafts, heavily connected footings) or flexible (thin rafts, loosely connected or disconnected footings).

For the specific case of lateral spreading, the continuity or mutual connection of foundation elements are the crucial features.

Based on these considerations, a simplified scenario of damage is considered in this work with reference to the most critical situation. A low reinforced concrete structure with isolated plinths, founded on a crust layer subjected to lateral spreading due to the liquefaction of the underlying saturated sand layer, is modeled (Fig. 1a). Due to the lateral spreading movement, all footings (except one) of a multiple frame are moving uniformly and the exterior footing has differential movement due to a soil crack. Then, the simplified structural mechanism considered in Fig. 1b will take place, and the right pillar will bend outwards. Depending on the number of storey and bays as well as on the characteristics of the multiple frame, all the elements of the structure will be subjected to lower stresses than the exterior pillar. A number of additional analyses, for different typical structural schemes (not shown here for the sake of brevity) supports this statement. For this reason, the structural model will be focussed on the exterior pillar only. Assuming that the frame has multiple storeys, which would prevent beam elongation and joint rotation, the exterior column will be considered fixed at top. However, beam elongation and joint rotation would reduce the chord rotation demand only slightly and not change the failure mechanism.

The structural scheme may represent a two storey two bays frame building.

The idea that the structural damage is concentrated in the columns rather than in the beams, is due to the fact that the columns are free to rotate laterally and therefore act as a
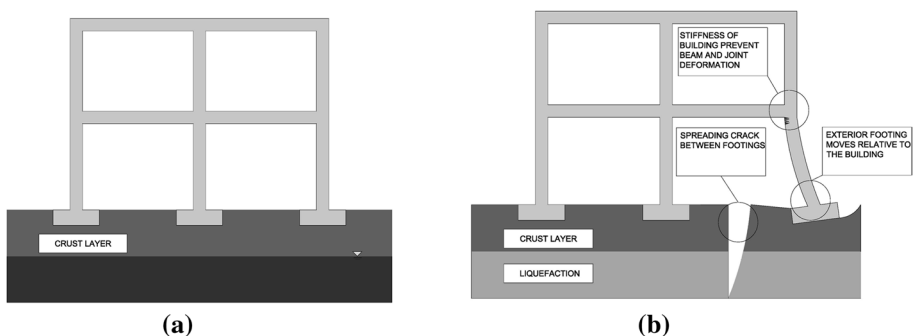

Fig. 1 R.C. structure on shallow foudations (**a**), Worse case scenario of damage due to lateral spreading (**b**)

cantilever in simple bending (Fotopoulou et al. 2018; Bird et al. 2006). This kind of defor-mation was confirmed by a CBF steel structure on shallow foundations affected by multiple cracks between the columns due to lateral spreading during the Kaikoura Eartquake (Mw 7.8). As it is possible to see from the Fig. 2 the columns of the structure are loaded hori-zontally by the differential soil movements due to the multiple cracks. For this reason the major deformations and thus the damages are concentrated in the columns rather than in the beams.

There is almost always a vertical component to lateral spreading. Although the pres-ence of a vertical component was found to influence the deformed shape of the structure, the amplitude of the horizontal foundation deformation was found to govern the damage state (Bird et al. 2005): i.e., given that vertical ground deformation occurs, and making the reasonable assumption that, during the Lateral Spreading phoenomenon, it will be less than the horizontal component, its actual amplitude is not required. This finding is compat-ible with the fact that most assessment methodologies tend to consider only the horizon-tal compenent (with the exception of Shamoto et al. 1998a, b), and therefore the vertical component of lateral spreading is less easily predicted. However, it is also noted that this simplification of lateral spreading to horizontal component only may lead to over-estimates of the movement, as shown by Cetin et al (2002). Therefore the amplitude of the vertical component, is not needed, since the horizontal foundation deformation govern the damage state during the lateral spreading phoenomenon.

In these hypotheses, the soil-structure interaction at the foundation level is taken into account with a simple displacement-based spring model (Fig. 3), following the approach proposed by Cubrinovski et al (2009). The known horizontal ground displacement repre-senting the differential free-field ground movement, Δ_{dem}, is applied at the free end of the soil spring, attached on the other side to the foundation of the column. Because of this, the foundation is loaded and moves horizontally by a quantity due to the structure, Δ_{str}, whose value will depend on the increment in demand Δ_{dem} as well as on the mechanical behav-iour of the deforming pillar, as sketched in the scheme of Fig. 3. The shortening of the soil spring Δ_{soil} is given by:

$$\Delta_{soil} = \Delta_{dem} - \Delta_{str} \tag{1}$$

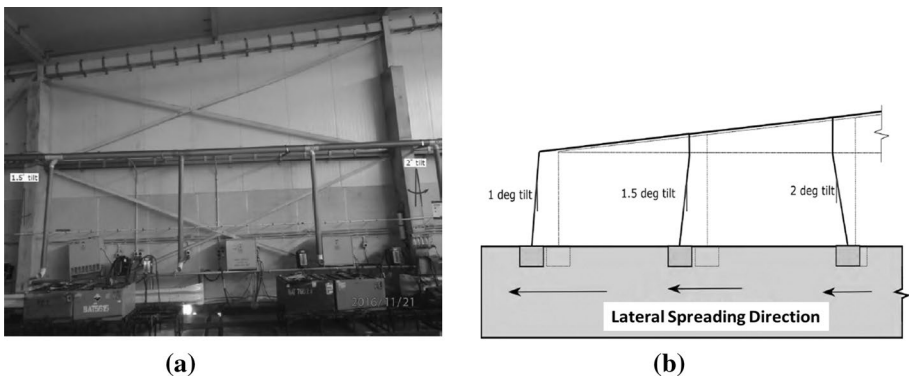(a)   (b)

Fig. 2 Damages on concentric braced frames steel structure on shallow foundation (**a**), Schematic of defor-mation pattern of steel frame along the building (**b**) (modified after GEER surveys)
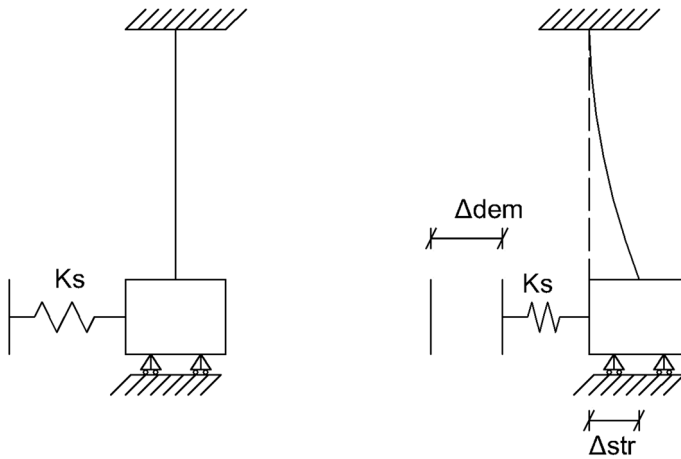
Fig. 3 Reinforced concrete macro-element fixed at the top with simple soil-spring model

Then, the horizontal force, F_{soil}, produced on the side of the foundation by the displacing ground can be calculated once a constitutive relationship $\Delta_{soil} - \sigma_{h,soil}$ is given, and the area A_f of the loaded side of the foundation is known ($A_f = h_f\, w_f$, where h_f and w_f are respectively the embedded height and the width of the foundation).

Because of equilibrium of horizontal forces, the force acting at the base of the pillar will match the force applied on the foundation by the soil ($F_{str} = F_{soil}$).

With this approach, the studied structure can be seen as a simple 2D reinforced concrete macro-element fixed at the top.

In this study the footing settlement has implicitly been considered, since in the case of extensive soil subsidence the footing would detach thus moment induced in the top of the column due to imposed gravity loads would reduce to zero as the beam would act as a cantilever, this is the critical case for the exterior column during the Lateral Spreading, as otherwise the gravity induced moment would produce favourable loads for the column (Fig. 4).

However, the reduced moment is transferred to the interior columns and beams which may reduces their capacity to handle lateral soil loads but this case has not been considered since the distribution of the load depends on additional structural characteristics. Note that in previous studies vertical displacements have been imposed directly to footings, suggesting differential settlement to be a critical loading condition for stiff frames, however, recent work by Gomez-Martinez et al. (2019) has shown this modelling approach to be highly conservative and not consistent with field observations from Cubrinovski et al. (2012) from the Christchurch earthquakes.

2.2 Constitutive models

A simple linear elastic—perfectly plastic behaviour is assumed for the soil spring between the displacement Δ_{soil} and the stress $\sigma_{h,soil}$, fully defined by two parameters: the stiffness k_s (in kN/m^3, that can be seen also as a subgrade reaction coefficient) and the limit stress $\sigma_{h,lim}$ (in kPa). These parameters can be determined using conventional field test results, as SPT blow count, N_{SPT}, following the indications by Murashev et al. (2014).

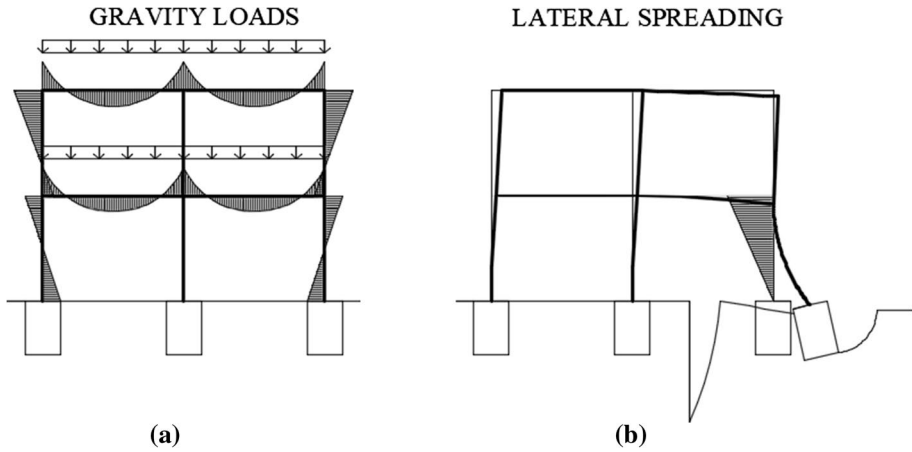GRAVITY LOADS   LATERAL SPREADING

(a)   **(b)**

Fig. 4 a Bending moment diagram due to the gravity loads on a two storey two bays frame structure; **b** bending moment diagram on the exterior column due to the lateral spreading load

With this approach, the stiffness k_s is expressed by the empirical and dimensional expression:

$$k_s = \frac{56 \cdot N_{spt}}{\left(100 \cdot w_f\right)^{\frac{3}{4}}} \tag{2}$$

The limit horizontal stress corresponds to the full mobilization of passive earth pressure ($\sigma_{h,lim} = \sigma_p$), and can be simply expressed using Rankine's formulation. Then, once the embedded loaded area $A_f = h_f \cdot w_f$ of the foundation is known, the $\Delta_{soil} - \sigma_{h,soil}$ relationship can be transformed into the $\Delta_{soil} - F_{soil}$ one. The two parameters of the $\Delta_{soil} - F_{soil}$ model are K_s and F_{lim}, expressed as:

$$K_s = k_s \cdot h_f \cdot w_f \tag{3}$$

$$F_{lim} = \alpha_f \cdot \sigma_p \cdot h_f \cdot w_f \tag{4}$$

The horizontal load applied to the foundation elements that the spreading soil applies, can be as high as 4.5 times the Rankine passive earth pressure (Cubrinovski et al. 2009). Obviously, this will depend on whether the soil moves past the foundation (typically in the case of fully liquefied soil) or a significant movement of the foundation occurs (typically when a crust of non-liquefiable material exists on top of the liquefied layer). The assessment requires a comparison between the passive soil forces imposed by the soil on the foundation versus the ultimate structural resistance (Cubrinovski et al. 2009).

As previously mentioned, a reinforced concrete frame is considered in this work. The displacing soil loads the foundation which in turn loads the pillar, modeled as a fixed cantilever. The concrete constitutive model is the simple so-called *stress-block* model, that uses a simplified rectangular equivalent diagram in compression and nil resistance to tension. The steel reinforcement is modeled considering an elastic-perfectly plastic stress–strain relationship. The bending moment M and the rotation Θ of the cantilever,

has threshold levels corresponding to the yielding of the reinforcement (Y) and to the ultimate state at concrete crushing (U).

The yield and ultimate chord's rotations ϑ_y and ϑ_u can be determined as (PrEN 1998-3):

$$\vartheta_y = \Phi_y \frac{L_v}{3} + 0.0013\left(1 + 1.5\frac{h}{L_v}\right) + 0.13\,\Phi_y\frac{d_b f_y}{\sqrt{f_c}} \tag{5}$$

$$\vartheta_u = \frac{1}{\gamma_{el}}0.016(0.3)^\nu\left[\frac{max(0.01;\omega')}{max(0.01;\omega)}f_c\right]^{0.225}\left(\frac{L_v}{h}\right)^{0.35}25^{\left(\alpha\rho_{sx}\frac{f_{yw}}{f_c}\right)}(1.25)^{100\,\rho_d} \tag{6}$$

The first term of the right side of Eq. (5) represents the flexural contribution, the second the contribution due to the effect of the shear stress and the third represents the contribution of the slip of the reinforcement steel bars.

The shear resistance V_R within the pillar cross section is expressed as (PrEN 1998-3):

$$V_R = \frac{h-x}{2L_v}\min\left(N, 0.55A_c f_c\right) + \left(1 - 0.05\min\left(5, \mu_\Delta^{pl}\right)\right)$$
$$\left[0.016\max(0.5, 100\rho_{tot}\left(1 - 0.16\min\left(5, \frac{L_v}{h}\right)\right)\sqrt{f_c}A_c + V_W\right] \tag{7}$$

The value of V_R is constant for $\vartheta \leq \vartheta_y$, and for larger values of ϑ it reduces up to a minimum value for $\vartheta = \vartheta_u$.

The meaning of the individual terms of the equations above is explained in "Appendix".

2.3 Soil-structure interaction mechanisms

In terms of the flexural behaviour of the pillar, according to EC8 the following limit states are considered in this paper:

- *Moderate damage state*, corresponding to the achievement of the yielding rotation ϑ_y in a section of a structural element.
- *Life safety limit state*, corresponding to the achievement of ¾ of the ultimate rotation ϑ_u in the section of a structural element.
- *Conventional collapse limit state*, which corresponds to the achievement of ultimate rotation ϑ_u or shear failure in a section of a structural element.

Depending on the characteristics in terms of strength and stiffness of the ground and of the structure, two different situations may take place, as depicted in Fig. 5. In the figure, the possible combinations of soil and pillar behaviour are plotted separately and also in a combined way, using Eq. 1. The two alternative situations are:

1. The soil limit force F_{lim} (Eq. 4) is smaller than $F_{str,y}$ ($= M_y/h_p$) then (Fig. 5a), whatever the value of Δ_{dem} (combined diagram), the structure is loaded in its elastic domain and is not damaged by ground lateral spreading.
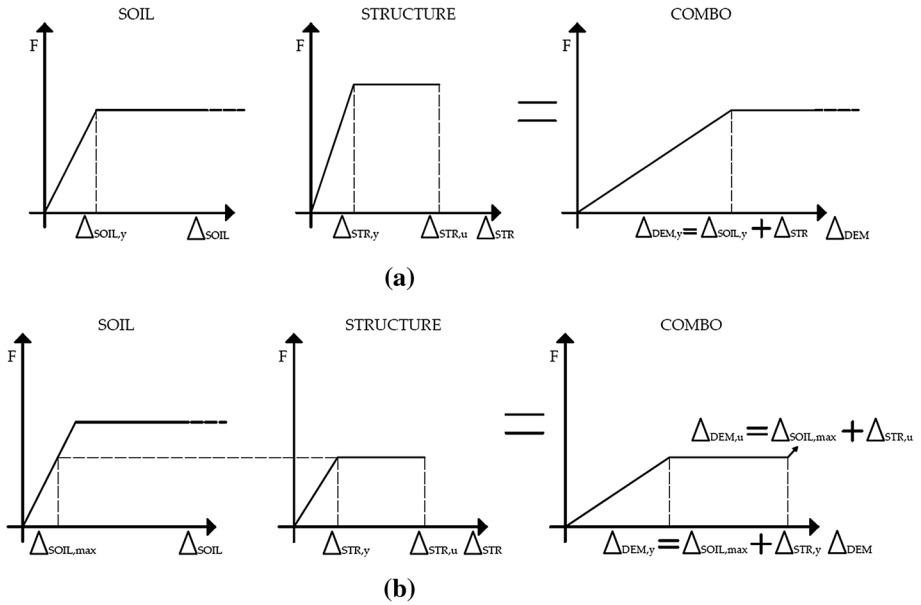
Fig. 5 Possible interaction mechanism. **a** Soil limit force F_{lim} is smaller than $F_{str,y}$; **b** soil limit force F_{lim} is higher than $F_{str,y}$

2. The soil limit force F_{lim} is higher than $F_{str,y}$; there is a value $\Delta_{soil,max}$ that induces on the structure the yielding force $F_{str,y}$ (Fig. 5b). For $\Delta_{soil} < \Delta_{soil,max}$, the structure will be loaded in its elastic range; for $\Delta_{soil} = \Delta_{soil,max}$ and $\Delta_{dem} > (\Delta_{soil,max} + \Delta_{str,y})$ the structure will be in a plastic range; while for $\Delta_{dem} = (\Delta_{soil,max} + \Delta_{str,u})$, the structure will collapse.

A routine was written in Python 3 to analyse the mechanism as follows: once Δ_{dem} is estimated, whatever the case considered in Fig. 5, it is possible to calculate the force F from the combined constitutive relationship and thus to calculate Δ_{str}, to check the structural behaviour.
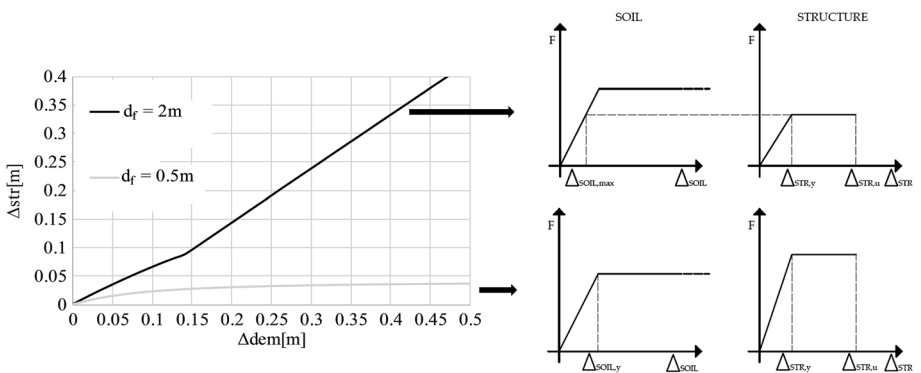

Fig. 6 Conceptual diagram when the soil yields and when the soil does not yield

To further clarify this concept, a Δ_{dem} vs. Δ_{str} chart is plotted in Fig. 6, in which the two different scenarios are plotted:

In the first scenario the soil is able to generate the yield of the structure. By increasing the input, it is possible to notice that the Δ_{str} also increases. This, as shown in the next sections, can happen for relevant depths of the foundation.

In the second scenario, the soil is not able to exert a pressure that yields the structure but reachs its maximum value and, given the infinitely-ductile behavior, it compresses indefinitely without compromising structural safety. That is why the differential displacement demand increases while the column displacement cannot.

With reason, focusing only on the damages induced by the Lateral Spreading phoenomenon, the effects associated to ground shaking were neglected. However, the damage associated to inertia demand in the building should be accounted for in considering the performance of building under lateral spreading conditions and in a simplistic manner can be considered using cracked section properties.

3 Parametric study

In order to identify the relative importance of all the factors affecting the problem, a parametric study was carried out by changing, in a range of reasonable values (Fotopoulou et al. 2018; Mariniello 2007; Negulescu and Foerster 2010) for two to five storeys low RC buildings, the pillar cross section, its percentage of reinforcement, the shear length of the pillar, the foundation depth, the soil unit weight, the soil friction angle (Table 1). The concrete cover, diameter and spacing of stirrups are assumed constant and equal to 40 mm, 6 mm and 150 mm, respectively.

In particular, carrying out a standard push-over analysis, each geometrical and geothecnical configuration was loaded with a differential horizontal displacements (Δ_{dem}) up to 0.5 m. In order to understand the influence of each individual parameter involved, the

Table 1 Reference value and variable parameters to create fragility cruves

| Reference value and variable parameters			
Parameter	Reference value	From–o	Distribution type
b-cross section	400 mm	300–450 mm	Linear increasing
h-cross section (h_c)	400 mm	300–450 mm	Linear increasing
Reinforced degree (R.degree)	0.75%	0.5–1%	Uniform
Δ_{dem}	0–0.5 m	0–0.5 m	Linear increasing
Shear length of pillar (L_v)	4 m	3–4.5 m	Uniform
Depth of foundation (d_f)	1 m	0.5–2 m	Uniform
Friction angle of soil	30°	Mean = 30; standard deviation = 3	Normal
Specific weight of soil	20kN/m³	19–21 kN/m³	Uniform
Height foundation (h_f)	0.5 m	0.3–1 m	Uniform
fc	20 N/mm²	Mean = 20; standard deviation = 6	Normal
fy	325 N/mm²	Mean = 325; standard deviation = 4.33	Normal
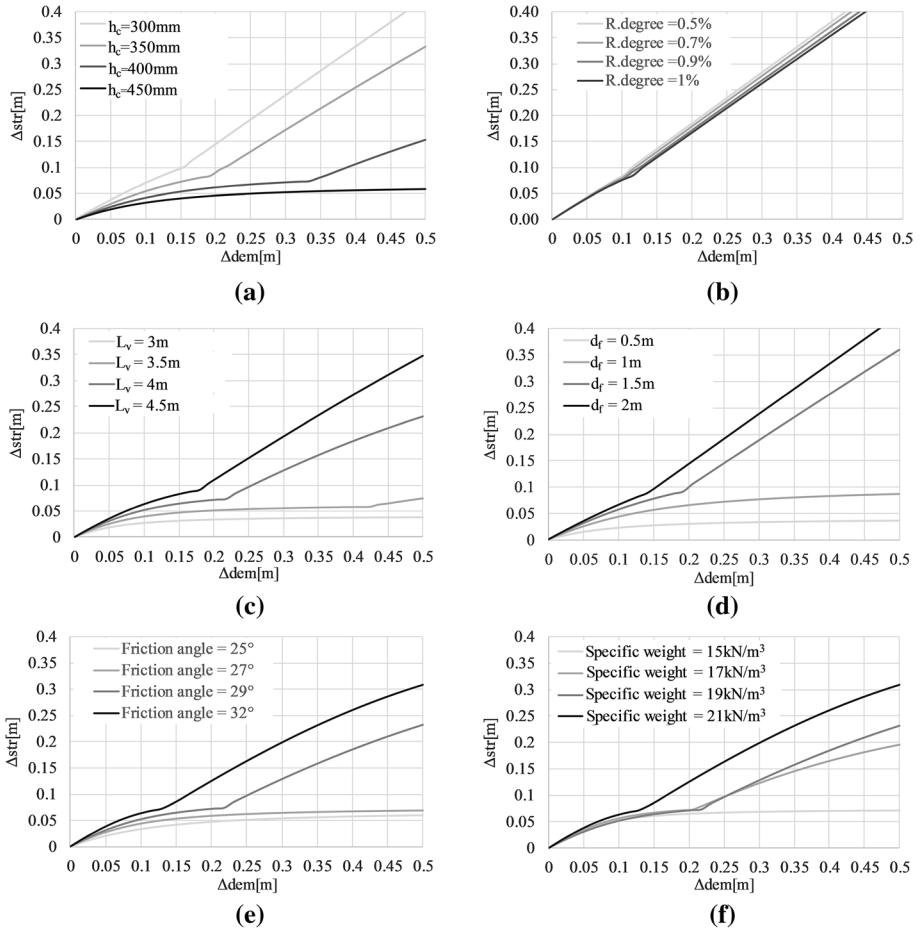
Fig. 7 a Varying only h-cross section; **b** varying only reinforcement degree; **c** varying only shear length; **d** varying only depth; **e** varying only friction angle; **f** varying only specific weight

reference values were used and, one by one, the studied parameters were varied linearly. Figure 7 summarizes the obtained results.

The parametric analysis indicates that the most relevant parameters are the height of the cross section of the pillar (h_c), the depth of the foundation (d_f) and the shear length of the pillar (L_v). The most critical situation is obviously the case of a slender pillar with a high foundation depth in a soil having a high friction angle. In the analysed range of values of the parameters, on the contrary, the degree of reinforcement in the pillar does not play a relevant role.

4 Vulnerability assessment

The simple numerical model described in Sect. 2 allowed the level of damage to be identified in a deterministic way. Assumptions were made on the parameters ruling the interaction mechanism and how they influence the capacity of the structure. In order to have results that may be of some practical usefulness, random variability and uncertainty should be taken into account. Indeed to capture the uncertainties associated with defining liquefaction-induced permanent ground deformations on a regional basis, a probabilistic approach is required (Bird et al. 2006). The variability of capacity and demand is generated introducing randomness in the parameters of the structural model as well as in those of the geotechnical one, with assigned probabilities given in the Table 1. These parameters represent, on the structural side, the low reinforced concrete buildings, while on the geotechnical one the loose sands. By using a Monte-Carlo simulation, different combinations of independent structural and geotechnical parameters are generated.

A fragility curve represents the probability that a defined class of buildings reaches a prefixed limit state for a given value of demand (Δ_{dem}, in this case).The process can be described according to the following formulation:

$$Fragility = \sum_{\Delta dem} P[C \leqslant D | IM = \Delta_{dem}] \tag{8}$$

For a given value of Δ_{dem}, therefore, the fragility curve expresses the percentage of buildings that exceeds a certain limit state or for which the capacity is lower than the demand. In order to generate the fragility curves the relative frequency method is used. The exceeding probability is approximated by the relative frequency, that is:

$$P_{ij} = n_{ij}/N \tag{9}$$

where n_{ij} is the number of cases found to exceed the capacity C_i, for a fixed value of demand j, among the performed N realizations. This is a crude, quite simple method characterized by being independent of any particular probability distribution of the realizations. In this work, fragility curves were produced using 2000 realizations. These probabilities can then be fitted into a curve (Fig. 8),usually representing the cumulative function of a normal distribution, as described by Shinozuka et al. (2000). The functional form is presented in Eq. 10:

Fig. 8 Fragility curves for reinforced concrete building with shallow foundations subject to lateral spreading
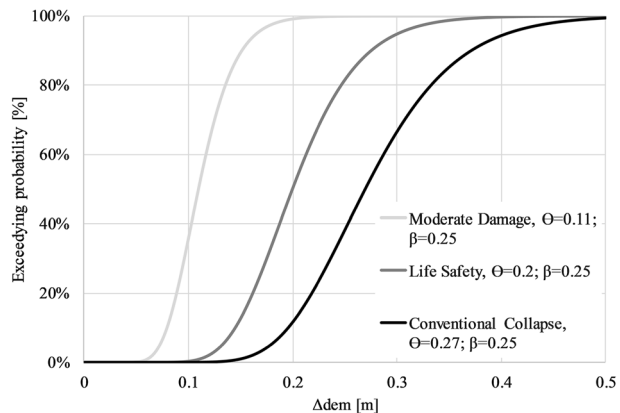
Table 2 Mean and standard deviation parameters computed for the three limit states proposed in this analysis, and used to build the fragility curves

Limit state	Mean (θ)	Standard deviation (β)
Moderate damage	0.11	0.25
Life safety	0.20	0.25
Conventional collapse	0.27	0.25

Fig. 9 Comparison of the proposed fragility curves subjected to differential settlements with the corresponding analytical ones of Bird et al. (2005)
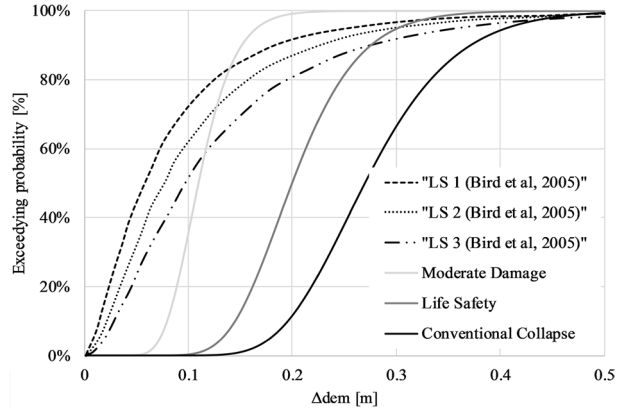
$$P(C|IM = x) = \Phi\left(\frac{\ln (x/\theta)}{\beta} \right) \tag{10}$$

where Φ () is the standard normal cumulative distribution function (CDF), θ is the median of the fragility function (the IM level with 50% probability of collapse) and β is the lognormal standard deviation of the IM (sometimes referred to as the dispersion of the Intensity Measure). The log-standard deviation parameter β describes the total dispersion related to each fragility curve. A higher β value leads to a flatter fragility curve and hence to greater uncertainty. The Maximum Likelihood Method is used to evaluate these statistical parameters. Equation 10 implies that the IM $= \Delta_{dem}$ values, causing the overcoming of the limit states, are lognormally distributed. The values of θ and β computed in this analysis are provided in Table 2.

5 Comparison with literaturae

The developed fragility curves for the studied low RC buildings are compared with some representative analytical fragility curves presented in Bird et al.(2005) for poor quality RC frames buildings sujected to differential horizontal foundation deformations. More specifically, Fig. 9 presents indicative comparisons between the herein curves derived for the low RC building subjected to lateral spreading and the corresponding ones taken from Bird et al. (2005) for damage states LS1, LS2 and LS3 which are featuring the same damage state definition as in this study.

Despite the large uncertainties involved in the problem, especially for high values of Δdem, a medium-slight agreement is observed for LSI while for LS2 and LS3 the analytical curves generally present much higher damage probability compared to the analytically derived curves of this study. A key reason for the above differences is the following: in Bird et al. (2005) the maximum differential displacement is assumed to be applied at the end of an edge column ($\Delta_{dem} = \Delta_{str}$) while in this study the fragility curves are derived accounting the SSI effect ($\Delta_{dem} \neq \Delta_{str}$). The computation of the SSI, and in particular the compression of the soil induced by the opening of the crack, has a beneficial effect on the structural damage. Summarizing, not all the Δ_{dem} will be applied at the end of the cantilever due to the soil compressibility.

6 Ground deformations induced by lateral spreading: field evidence in Christchurch

In the Christchurch area (New Zealand), where the land is relatively flat and covered by river and stream channels, lateral spreading was predominant during the Canterbury Earthquake Sequence (2010–2011) and caused severe land, infrastructure and building damage. The Canterbury Plains stretch along about 160 km of the South Island's central east coastline and extend about 50 km inland, making them New Zealand's largest stretch of relatively flat land. Near surface sediments of Christchurch urban area include sands, silts and clay deposited in a marine environment and gravel plus 'overbank' silts and sands deposited in a terrestrial environment. The depth to groundwater in the city is greatest in the west (at about 5 m) and decreases towards the coast to a depth of about 1 to 1.5 m throughout the eastern suburbs.
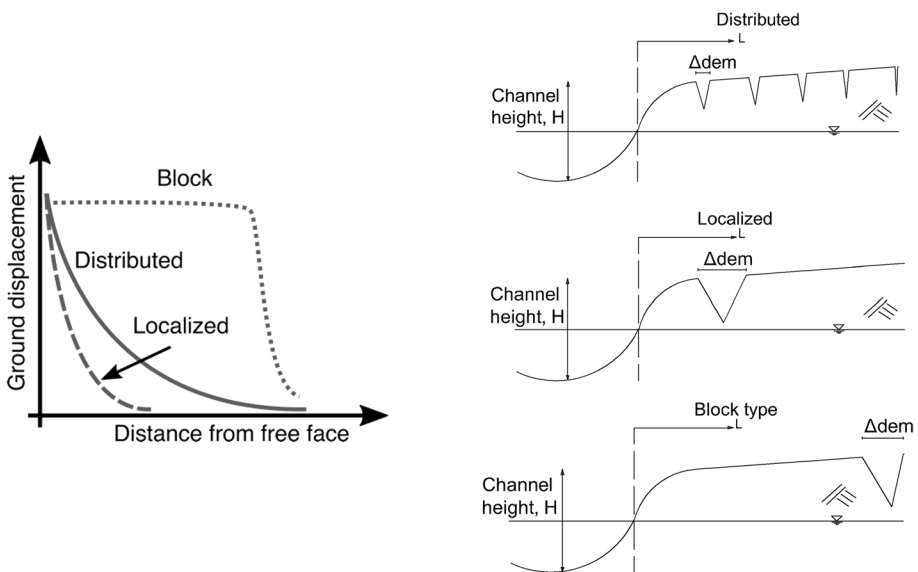

Fig. 10 Schematic various failure modes observed from ground surveying results. Adapted from Robinson (2016)

Three types of lateral spreading displacement patterns were indentified by Robinson (2016) from their ground survey data, as schematically depicted in Fig. 10:

(a) distributed pattern—cracks of decreasing width but more or less evenly distributed along the transect.
(b) localized pattern—large displacements (up to about 1.5 m) concentrated within about 30 m from the river, and no relevant displacements further from it.
(c) block pattern—few cracks with large relative displacements open at a significant distance from the river free-face (> 150 m) resulting in a block-like movement of the crust.

The "distributed" displacement pattern was the most common lateral spreading failure mechanism (Robinson 2016). The affected distances are typically within 100–150 m from the free-face but up to 250 m or more in some cases. The distributed type can be further subdivided into "large and distributed ground displacements", where the maximum displacements measured along the transects generally are larger than 0.6 m, and "moderate and distributed ground displacements" with maximum cumulative displacements ranging from about 0.3 to 0.6 m. Since "block" or "localized" mechanisms are characterized by a single, or just a few, large cracks concentrated in a small space, the probability that a structure would experience damage due to differential displacement is low. Therefore, in this work only the distributed pattern was considered and analyzed as a relevant hazard for structures.

In order to assess the magnitude of differential displacements that may produce damage to structures, a sample of nine large and distributed displacement profiles obtained by Robinson (2016) from ground survey after the 2010–2011 Canterbury Earthquake Sequence were analyzed. The ground surveys were taken either after the Darfield 2010 earthquake (df) or the Christchurch 2011 earthquake (ch), and, in two locations, after both, giving the nine transects in Fig. 11a from the seven locations shown in Fig. 11b. The dataset presented represents a mixture of demand from both a single event (Darfield 2010 only) and multiple events (Darfield 2010 and Christchurch 2011), thus reflecting that aftershocks and subsequent events can add to the demand felt on a building near a river.

The transects were collected using the detailed survey method, which has high accuracy with respect to capturing cracks and local movement compared to other techniques
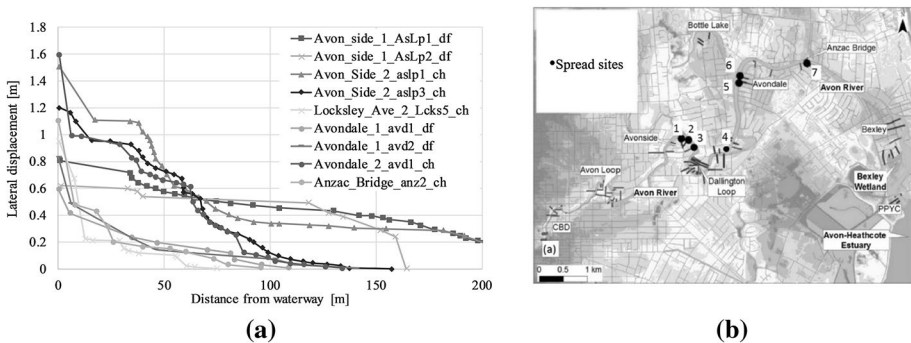

Fig. 11 **a** Results of ground survey at large and distributed spread sites and **b** location of large spread sites. Adapted from Robinson (2016)
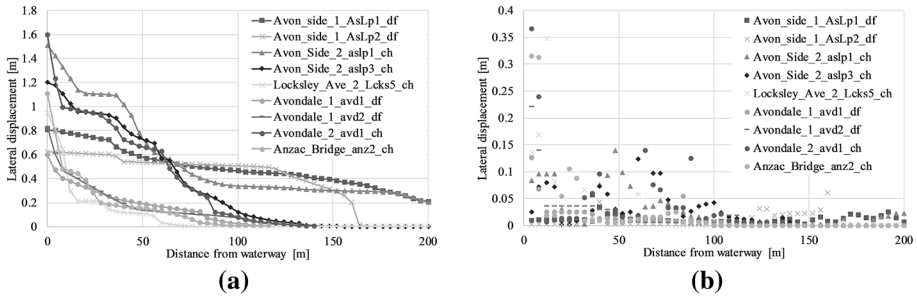
Fig. 12 **a** Lateral ground displacements (modified after Robinson 2016) and **b** corresponding relative displacement
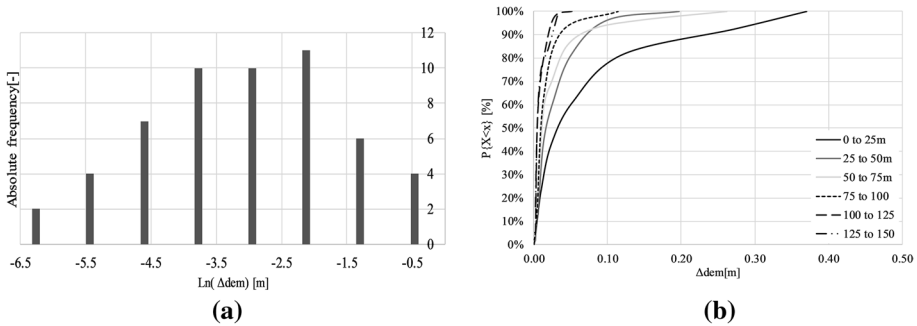

Fig. 13 **a** Histogram of absolute frequency for the soil closest to the river (distance 0–25 m); **b** cumulative density function for all intervals

(e.g. Lidar) but may generate cumulative error when estimating global displacements due to method summing up the cracks from the edge of a waterway (Robinson 2016). All of the sites were characterized by homogeneous topographic and stratigraphic characteristics such as relatively flat or gently sloping to the river (0–1.5%), channel heights (H) ranging from about 1.8 to 3.5 m, the presence of the loose fine to silty sand layer and the associated characteristics of this layer including:

- Liquefiable layer thickness greater than 1.5 m (1.6–2.7 m).
- Low resistance: $q_{c1} \sim 4$–7 MPa;
- Continuity of the loose fine to silty sand layer with distance from the bank at slopes of +0.9–6%;
- Continuity of the loose fine to silty sand layer along the bank;
- Loose fine to silty sand layer encountered at depths of 1.2–4 m.

To compute the differential displacement demand, the difference in ground displacement at 4 m intervals was computed from the available transects. The 4 m spacing represents the average spacing between columns in a low span framed building, thus assuming the calculated differential lateral ground displacement as the demand (Δ_{dem}) in the soil-structure interaction mechanism. Since the field data was available at different and variable spacings
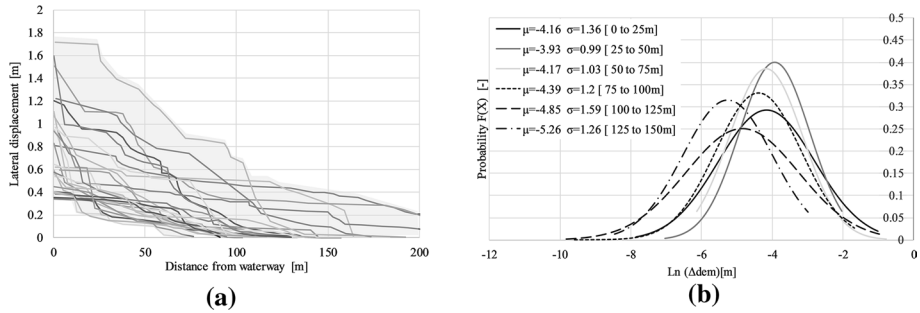
Fig. 14 **a** 32 Distributed displacement profiles; **b** PDF of 32 distributed displacement profiles

along each transect, a linear interpolation was done between subsequent data. Figure 12a shows the nine resampled profiles of lateral displacements in the area of interest, while Fig. 12b shows the corresponding differential displacement demand Δ_{dem}.

The dataset was subdivided in intervals of 25 m of distance, from the closest (0 m to 25 m) to the furthest (125 m to 150 m) from the river and frequency of occurrence for each subset was fitted with a lognormal probability density function. The histogram of absolute frequency for the interval [0, 25] m is shown in Fig. 13a and the cumulative probability for all subsets is shown in Fig. 13b. Consistent with literature indications, Fig. 13b shows a general trend of differential displacements decreasing for increasing distance from the waterway.

The process was repeated for 32 similar distributed displacement profiles collected by Robinson (2016), however, for these transects the topography and stratigraphy was nonuniform compared to the uniformity of the nine "large and distributed" profiles. The resampled profiles are shown in Fig. 14a and the fitted lognormal cumulative distribution functions are shown in Fig. 14b. The mean μ and standard deviation σ of the nine and the 32 profiles are compared in Table 3.

The results of the statistical interpretation of the patterns in terms of average and standard deviation are significantly different (Table 3), reflecting the complexity of the lateral spreading phenomenon and the the necessary connection with the topographic and stratigraphical conditions. Unfortunately, to the best of the authors knowledge, there are currently no available simple methods for estimating the differential lateral spreading displacement. Existing lateral spreading methods (e.g. Youd et al. 2002a, b, Zhang et al. 2004)) have focused on the estimation of the total displacement and tend to smooth out the block type movements that accentuate differential displacements. In the

Table 3 Comparison of mean and standard deviation

Distance	9 profiles		32 profiles	
	μ (m)	σ (m)	μ (m)	σ (m)
[0–25 m]	−3.67	1.6	−4.16	1.36
[25–50 m]	−4.12	1.15	−3.93	0.99
[50–75 m]	−4.32	1.11	−4.17	1.03
[75–100 m]	−4.73	1.25	−4.39	1.2
[100–125 m]	−5.23	0.88	−4.85	1.59
[125–150 m]	−5.17	0.91	−5.26	1.26

Fig. 15 Approximate Δ_{dem} at a given distance from the waterway
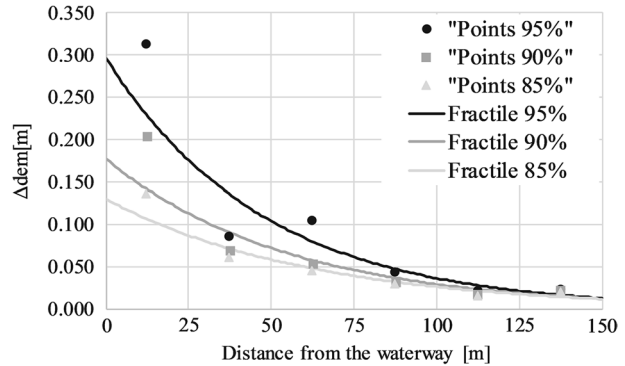

Table 4 Hazard matrix—differential displacement demand with distance from the river

Hazard matrix

Fractile (%)	[0–25 m] (m)	[25–50 m] (m)	[50–75 m] (m)	[75–100 m] (m)	[100–125 m] (m)	[125–150 m] (m)
95	0.31	0.09	0.10	0.04	0.02	0.02
90	0.20	0.07	0.05	0.03	0.02	0.02
85	0.14	0.06	0.04	0.03	0.02	0.02

following risk assessment only the demands associated with the nine transects on which detailed soil information were available have been considered.

The field data reported in this paper indicate that the ground differential settlements caused by lateral spreading follow a log normal probability distribution (Fig. 13). Then, for each interval of distances from the waterway considered in Fig. 13, the value of Δ_{dem} corresponding to a given fractile (i.e. to a given risk level) can be calculated, and curves $\Delta_{dem}(x)$ can be plotted for different risk levels (Fig. 15).

These curves, with their respective values, represent the action (imposed displacement) to which the structure would be subjected to.

Table 4 shows the fractile values of hazard that have been considered in the following risk study.

7 Evaluation of risk at different distances from waterway

The differential displacement demand, Δ_{dem} is highly uncertain because of the limited available information and lack of methods for estimating it. Instead the case study results from the Avon River (Fig. 15) have been used in this assessment. By combining the demand information from the Avon River that expresses the demand as a function of the

Fig. 16 Risk varying distance from the river with fractile 95%
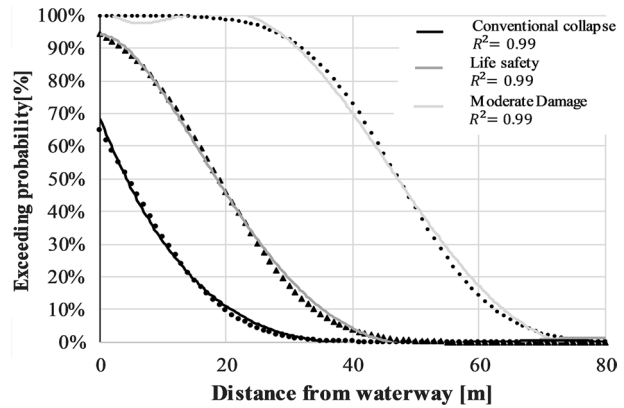
distance from the river for a given risk level, with the fragility curves (Fig. 8), it is possible to investigate what is the probability of overcoming the various limit states at different distances from the river, for a given risk level.

In this case, assuming a risk level of 5% (i.e. a fractile equal to 95%), as the distance from the river increase, it is possible to intersect the fragility curves with a values of Δ_{dem} and returns the probability of exceeding the various limit states. By using a polynomial interpolation it is possible to compute the best fitted curves of the probability points. The results reported in Fig. 16 were obtained.

These results allow, for a risk level of 5%, a quantitative estimate of the probability of attaining one of the three considered limit states (moderate damage, life safety, structural collapse) in a concrete framed structure founded on isolated shallow foundations because of lateral spreading, at different distances from the waterway towards which the soil is moving.

8 Extension of the methodology to a new site

When faced with significant uncertainty in the process of making a forecast or estimation, rather than just replacing the uncertain variable with a single average number, the Monte Carlo Simulation might prove to be a better solution. In order to extend the procedure to a new site, it is possible to use this kind of approach. The Youd et al. analytical formulation (2002a, b) can be used to perform a Montecarlo simulation:

$$\log(D_h) = -16.713 + 1.532M - 1.40R^* - 0.012R + 0.592\log(W)$$
$$+ 0.540\log(T_{15}) + 3.413\log(100 - F_{15}) - 0.795\log(D50_{15} + 0.1)$$

(11)

- D_H = Estimated lateral ground displacement, in m.
- $D50_{15}$ = Average mean-grain size in granular layers included in T15, in mm.
- F_{15} = Average fines content (fraction of sediment sample passing a No. 200 sieve) for granular layers included inT15, in percent.
- M = Earthquake magnitude (moment magnitude).

Parameter	Probability distribution	From–to
M	Uniform	Min = 6.3 Max = 7.1
T_{15}	Uniform	Min = 1 m Max = 4 m
F_{15}	Normal	Mean = 25% Standard deviation = 6.5%
$D50_{15}$	Fixed	0.19 mm
R	Fixed	17 km
H	Fixed	3 m

Table 5 Geotechnical and seismic hazard parameters for the 7 spread sites considered, during the Canterbury earthquake sequence (2010–2011)

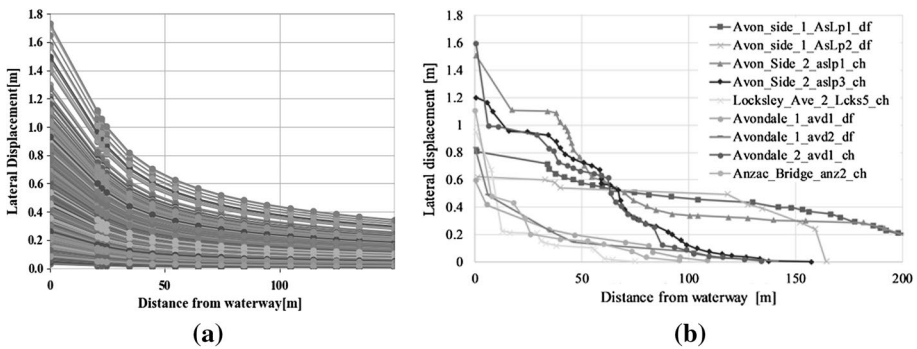- $R =$ Horizontal distance from the seismic energy source, in km.

Fig. 17 a Lateral spreading profiles derived by the Monte-Carlo simulation; **b** lateral spreading profiles derived by ground surveys

- $T_{15} =$ Cumulative thickness of saturated granular layers with corrected blow count, (N1) 60 less than 15, in m.
- $W =$ Ratio of the height (H) of the free face to the distance (L) from the base of the free face to the point in question, in percentage.

To generate a great number of scenarios, it is possible to assign a probability distribution (normal, log normal, uniform) to some parameters of the Youd et al. formulation. The choice of a particular probability distribution and their parameters (mean, standard deviation) derives from geotechnical and seismic investigations of the new site. Moreover, considering a specific hazard, it will be also possible to assign a probability distribution to the distance from the epicentre (seismic source). By linearly varying the free face-ratio up to a distance of 150 m from the river it will be possible to generate the lateral spreading profiles for a new site and then apply the method as stated before.

In order to validate the outlined procedure, the empirical lateral spreading profiles considered in Fig. 11 were compared with the lateral spreading profiles obtained thorough the Monte-Carlo simulation. One thousand lateral spreading profiles have been generated thorough the Monte-Carlo simulation using the parameters reported in Table 5 (Fig. 17a). These parameters reflect the geotechnical and seismic condition where the 9 profiles of Fig. 11 were investigated (Robinson 2016).
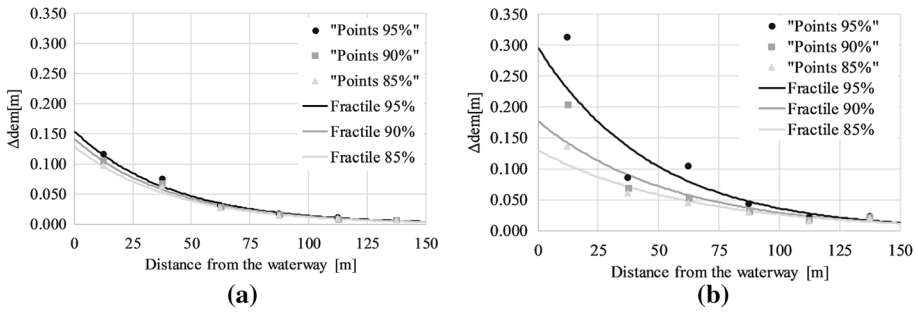
Fig. 18 **a** Approximate Δ_{dem} at a given distance derived by the Monte-Carlo simulation; **b** approximate Δ_{dem} at a given distance derived by ground surveys

Once all displacement profiles have been defined, the difference of horizontal displacement between points that have a consecutive distance of 4 m, up to a distance from the river of 150 m, has been computed. Therefore, repeating the procedure and taking into account the 95%–90%–85% fractile curve, it is possible to generate the demand curves as the distance from the river changes (Fig. 18a).

The shown procedure under predicts lateral stretch for the Christchurch case (Fig. 18a, b), but can be accounted for by multiplying the lateral stretch values by ~ 2. This coefficient is in line with the fact that the empirical procedures used for estimating liquefaction-induced lateral displacements are generally accepted to be accurate only within a factor of 2 or 3 (Bird et al. 2006).

9 Validation case studies

To validate the simple mechanism-based modelling procedure a series of different buildings that experienced lateral spreading during the Haiti 2010, Darfield NZ 2010 and Christchurch NZ 2011 and Kaikoura NZ 2016 earthquakes were evaluated in terms of damage manifestation. Each building has been evaluated in Table 6 in terms of the structural resistance, the foundation type, the lateral stretch (Δ),the extent of damage and the type of mechanism developed. The peak ground acceleration (PGA) and distance to the free-face (Lff) have also been included to provide context on the expected shaking damage and lateral spreading potential (Table 6).

From Table 6 it can be seen that when the lateral stretch is significant (greater than 0.2 m) then the weak structures developed a structural mechanism such that the building was essentially torned apart (e.g. Fig. 20 of building No. 2), whereas in the case of strong structural resistance either the displacement was not sufficient or the soil mechanism was developed (Figs. 19, 20, 21).

It is possible to group the buildings in three categories (Table 7).

It is clear that where the perimeter and internal foundation walls beneath the building were strongly tied together and acted as a diaphragm, effectively prevent differential horizontal movements between structural elements. The bucking of the concentric frames (see Figs. 2, 22) shows the attempt of the structure to prevent differential horizontal movement.

One may object that this difference is also due to the different lateral spreading profiles which each building is subjected but specially for the structure n°1–14 the distance from the free-face (key factor in evaluation of Lateral Spreading displacement) is minimal and

Table 6 Considered case studies with the indication of the structural typology, foundation type, lateral stretch, damage observed, mechanism developed, PGA, distance from free-face

No.	Description	Structure	Foundation	Δ (m)	Damage	Mechanism	PGA (g)	L_{ff} (m)
1	Warehouse in Port-au-Prince, Haiti[a]	STRONG—Metal- Steel	Perimeter strip	~0.2–0.3	MEDIUM	Not developed	0.2	20
2	Residence in Kaiapoi South, NZ[b]	WEAK—Light wood framing	Unreinforced slabs, perimeter stem wall	~1	HEAVY (SPLIT)	Full Structural	0.19	200
3	Residence in Kaiapoi South, NZ[b]	WEAK—Light wood framing	Unreinforced slabs, perimeter stem wall	~1.5	HEAVY (SPLIT)	Full Structural	0.19	200
4	Residence in Dallington, NZ[b]	WEAK—Bond brick perimeter walls with light metal roofs	Unreinforced slabs, perimeter stem wall	~0.1–0.2	MEDIUM	Structural	0.2	81
5	Residence in Dallington, NZ[b]	WEAK—Bond brick perimeter walls with light metal roofs	Unreinforced slabs, perimeter stem wall	~0.1–0.2	MEDIUM	Not developed	0.2	140
6	Residence in Dallington, NZ[b]	WEAK-Light wood framing along longitudinal axes and brick along their transverse axes	Unreinforced slabs, perimeter stem wall	~0.1–0.2	MEDIUM	Not developed	0.2	145
7	Residence in Dallington, NZ[b]	WEAK—Light wood framing along longitudinal axes and brick along their transverse axes	Unreinforced slabs, perimeter stem wall	~0.1–0.2	MEDIUM	Not developed	0.2	145
8	Residence in Dallington, NZ[b]	WEAK—Light wood framing along longitudinal axes and brick along their transverse axes	Unreinforced slabs, perimeter stem wall	~0.1–0.2	MEDIUM	Not developed	0.2	150
9	Residence in Dallington, NZ[b]	WEAK—Masonry block units	Unreinforced slabs, perimeter stem wall	~0.1–0.2	MEDIUM	Not developed	0.2	145
10	Residence in Spencerville, NZ[b]	WEAK—Slab foundations probably with light wood framing	Unreinforced slabs, perimeter stem wall	~0.4–0.5	HEAVY (SPLIT)	Full Structural	0.17	45
11	Residence in Spencerville, NZ[b]	WEAK—Slab foundations probably with light wood framing	Unreinforced slabs, perimeter stem wall	~0.4–0.5	HEAVY (SPLIT)	Full Structural	0.17	50

Table 6 (continued)

No.	Description	Structure	Foundation	Δ (m)	Damage	Mechanism	PGA (g)	L_{ff} (m)
12	Residence in Bexley, NZ[b]	WEAK -Slab foundations probably with light wood framing	Unreinforced slabs, perimeter stem wall	~0.4–0.5	HEAVY (SPLIT)	Full Structural	0.19	40
13	Building in CBD, NZ[c]	STRONG—Reinforced concrete frames	RC shallow foundation	~0.15	MODERATE	Soil	0.45	120
14	Shed in Wellington port, NZ[d]	STRONG -CBF steel	Composite shallow foundation with RC spread footings and mats	~0.2	MODERATE	Soil	0.235	20

[a]GEER (2010a), GEOTECHNICAL ENGINERRING RECONNAISSANCE OF THE 2010 HAITI EARTHQUAKE
[b]GEER (2010b), GEOTECHNICAL RECONNAISSANCE OF THE 2010 DARFIELD (NEW ZEALAND) EARTHQUAKE
[c]GEER (2011), GEOTECHNICAL RECONNAISSANCE OF THE 2011 CHRISTCHURCH, NEW ZEALAND EARTHQUAKE
[d]GEER (2012), GEOTECHNICAL RECONNAISSANCE OF THE 2016 Mw7.8 KAIKOURA, NEW ZEALAND EARTHQUAKE
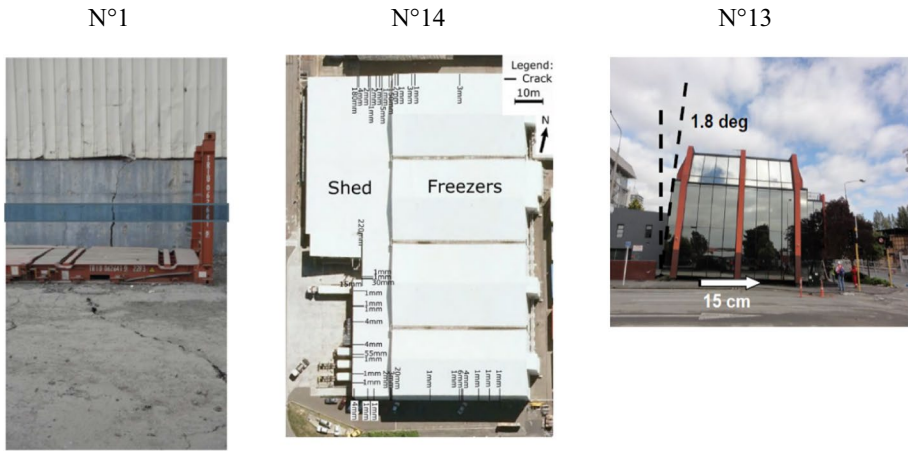
N°1   N°14   N°13

Fig. 19 Buildings A. Stiff structures where the structural mechanism is not developed

N°2   N°3   N°10

N°11   N°12

Fig. 20 Buildings B. Weak structures where the structural mechanism is developed

the P.G.A is about the same for all the buildings (Table 6). Assigning a level of damage from 1 (moderate) to 3 (heavy—completely split) it is possible to see that the structures able to prevent the horizontal differential movement induced by the lateral spreading have

N°5 N°9

Fig. 21 Buildings C. Brick and Masonry Structures where the lateral stretching was inable to generate a well defined soil or structural mechanism

Fig. 22 Buckling of the CBF steel structures due to the stiffness of the structures

Table 7 Categories of structures with different mechanisms developed

| Categories	Description
Buildings A	The structural stiffness was sufficient to resistance the lateral spreading load and thus only minor structural distortion was observed (structures n°1–13–14)
Buildings B	The structures with only light timber framing were weak and the footing displacements were close to the ground movements thus large structural distortion was observed (structures n°2–3–10–11–12)
Buildings C	The brick and masonry structures due to their low tensile strength showed separation of brick–mortar joints (n°4–5–6–7–8–9) even if the lateral stretching was light (10–20 mm). However the lateral stretching was inable to generate a well defined soil or structural mechanism
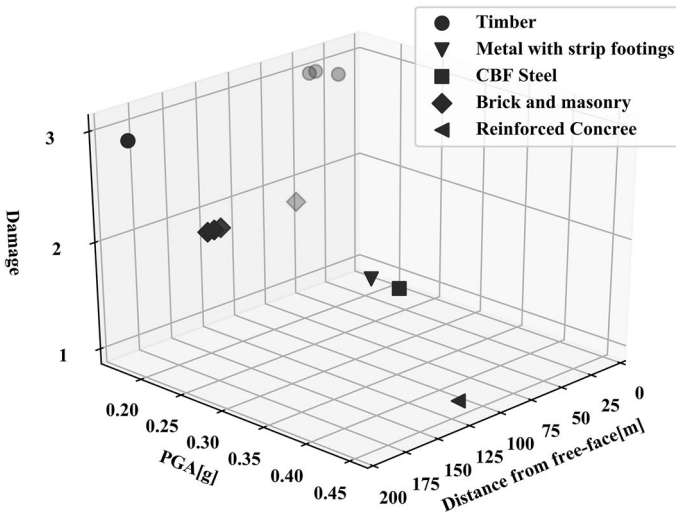
Fig. 23 Case studies analyzed with the reported damaged, distance from Free-Face, PGA

reported minor damage than the timber and masonry ones even if the latter were much more distant from the free-face and therefore subject to less distortion (Fig. 23).

10 Conclusion

This paper has introduced a simple procedure to estimate the risk of attaining a limit state in a framed structure on shallow foundations due to liquefaction induced lateral spreading. A simple 2D macroelement was adopted to account for soil structure interaction, and fragility curves were produced for two to five storeys reinforced concrete building on shallow foundations based on a large number of calculations, taking into account the random variability of the relevant mechanical and geometrical parameters. The field measurements reported in Robinson (2016) were used to quantify the likely differential lateral spreading displacements along the Avon River during the Canterbury Earthquakes Sequence (2010–2011). For the considered building and displacement demands, the risk assessment indicated that the risk of collapse from lateral spreading is relevant in the first 40 m away from the river; for higher distances, only the limit state of moderate damage may be attained.

It may be argued that the adopted model is too simple to be representative for a real class of buildings, and that the possibility of global tilting and complex loading due to vertical differential dispacements was not taken into account. Nonetheless, such a simple model is useful as it allows to estimate, in a regional scale preliminary assesment, the vulnerability to the lateral spreading. Furthermore, the outlined procedure is able to highlight the key parameters ruling the risk connected to cracks opening because of lateral spreading, leading to a better understanding of the soil-structure interaction mechanism for shallow foundations under these conditions. It has to be also highlighted that in this work different interaction mechanisms were considered, depending on soil friction angle and the geometric features of the pillar and the foundation. By explicitly taking into account soil constitutive behaviour, in fact, it has been shown that damage caused by lateral spreading

would be largely overestimated by overlooking soil structure interaction and simply applying the expected horizontal displacement demand directly to the structure. The simplicity of the procedure easily allows the variation of materials to be consider for the application in regional based loss assessment. Future work could be oriented towards the extension of the procedure on a full structural models with soil-structure interaction.

Appendix

Parameters

d_b	Diameter of longitudinal reinforced steel bars
d_f	Depth of foundation
f_c f_y f_{yw}	The compressive strength of concrete and longitudinal and trasversal yield steel
h_c	Height of the cross section
h_f	Height of foundation
k_s	Soil spring stiffness
L_v	Distance between the point at maximum moment and the point at zero moment on an element. In this case it is equal to the length of the pillar
N_{spt}	SPT blowcount
V_w	Contribution of transversal bars
w_f	Width of the foundation
x	Neutral axis
α	Factor of confinement efficiency. It is possible to assume this value equal to 0 for existing buildings
α_f	Factor to account for the 'wedge-effect' of increased pressure on a single pile or isolated shallow foundation in comparison to an equivalent wall
γ_{el}	Coefficient equal to 1.5 for primary elements
Δ_{dem}	Horizontal ground displacement representing the differential free-field ground movement
Δ_{soil}	Shortening of the soil spring
Δ_{str}	Horizontal structural displacement due to the load of the soil
$\mu_\Delta^{pl} = \frac{\theta - \theta_y}{\theta_y}$	Coefficient that reduces the shear resistance as the demand increases in the plastic range
$v = \frac{N}{Ac*fc}$	Normalized axial force of compression acting on the whole Ac section
p_d	Percentage of any diagonal armor
$p_{sx} = \frac{A_{sx}}{b_w*s_h}$	The percentage of transversal reinforcement with s_h spacing between the stirrups
$p_{tot} = \frac{A_s + A'_s}{b*h}$	Geometrical reinforced steel percentage of cross section
σ_p	Rankine passive pressure
$y = \frac{2\varepsilon_{sy}}{h - 2c}$	Yield curvature from cross section deformation equilibrium
$\omega = \frac{A's*fy}{Ac*fc}$	Mechanical percentages of longitudinal reinforcement in traction
$\omega' = \frac{As*fy}{Ac*fc}$	Mechanical percentages of longitudinal reinforcement in compression

References

Bardet JP, Seed RB, Cetin KO, Lettis W, Rathje E, Rau G, Seed RB, Ural D, Baturay MB, Boulanger RW, Bray JD (2000) Soil liquefaction, landslides, and subsidences. Earthq Spectra 16(S1):141–162. https://doi.org/10.1193/1.1586151

Bartlett SF, Youd TL (1992) Empirical analysis of horizontal ground displacement generated by lique-faction-induced lateral spread. Technical report NCEER-92-0021

Bird JF, Crowley H, Pinho R, Bommer JJ (2005) Assessment of building response to liquefaction-induced differential ground deformation. Bull NZ Nat Soc Earthq Eng 38(4):215–234

Bird JF, Bommer JJ, Crowley H, Pinho R (2006) Modelling liquefaction-induced building damage in earthquake loss estimation. Soil Dyn Earthq Eng 26:15–30. https://doi.org/10.1016/j.soildyn.2005.10.002

Boscardin MD, Cording EJ (1989) Building response to excavation-induced settlement. J Geotech Eng 115(1):1–21

Bouckovalas GD, Tsiapas YZ, Theocharis AI, Chaloulos YK (2016) Ground response at liquefied sites seismic isolation or amplification. Soil Dyn Earthq Eng. https://doi.org/10.1016/j.soildyn.2016.09.028

Boulanger RW, Mejia LH, Idriss IM (1997) Liquefaction at moss landing during Loma prieta earthquake. J Geotech Geoenviron Eng ASCE 123(5):453–467

Cetin KO, Youd TL, Seed RB, Bray JD, Sancio R, Lettis W, Yilmaz MT, Durgunoglu HT (2002) Lique-faction-induced ground deformations at Hotel Sapanca during Kocaeli (Izmit), Turkey earthquake. Soil Dyn Earthq Eng 22:1083–1092. https://doi.org/10.1016/S0267-7261(02)00134-3

Cetin KO, Youd TL, Seed RB, Bray JD, Stewart JP, Durgunoglu HT, Lettis W, Yilmaz MT (2004) Liq-uefaction-induced lateral spreading at Izmit Bay during the Kocaeli (Izmit)-Turkey earthquake. J Geotech Geoenviron Eng ASCE 130(12):1300–1313

Comartin CD, Greene M, Tubbesing SK (eds) (1995) The Hyogo-ken Nanbu earthquake, January 17, 1995. Preliminary reconnaissance report, Earthquake Engineering Research Institute

Cubrinovski M et al (2009) Pseudo-static analysis of piles subjected to lateral spreading. Bull N Z Soc Earthq Eng 42(1):28–38

Cubrinovski M et al (2012) Lateral spreading and its impacts in urban areas in the 2010–2011 Christch-urch earthquakes. N Z J Geol Geophys 55:255–269. https://doi.org/10.1080/00288306.2012.699895

Cubrinovski M, Bray JD, de la Torre C, Olsen M, Bradley BA, Chiaro G et al (2018) Liquefaction-induced damage and CPT characterization of the reclamations at CentrePort, Wellington. Bull Seis-mol Soc Am 108(3B):1695–1708. https://doi.org/10.1785/0120170246

EN 1998-3 (2005) Eurocode 8: design of structuresfor earthquake resistance—part 3: assessment and retrofitting of buildings

Faris A, Seed RB, Kayen RE, Wu J (2006) A semi-empirical model for the estimation of maximum horizontal displacement due to liquefaction-induced lateral spreading. In: Proceedings, 8th U.S. national conference on earthquake engineering, paper 1323

Fotopoulou S, Karafagka S, Pitilakis K (2018) Vulnerability assessment of low-code reinforced concrete frame buildings subjected to liquefaction-induced differential displacements. Soil Dyn Earthq Eng 110:173–184. https://doi.org/10.1016/j.soildyn.2018.04.010

Gomez-Martinez F, Millen MDL, Costa PA, Romão X (2019) Estimation of the potential relevance of differential settlements in earthquake-induced liquefaction damage assessment. Eng Struct 1–38 (in production)

Hamada M, Wakamatsu K (1998) Liquefaction-induced ground displacement triggered by quaywall movement. Soils Found Spec Issue 2:85–95

Hamada M, Towhata I, Yasuda S, Isoyama R (1987) Study of permanent ground displacement induced by seismic liquefaction. Comput Geotech 4:197–220

Holzer TL (ed) (1998) The Loma Prieta, California, earthquake of October 17, 1989— Liquefaction, U.S. Geological Survey Professional Paper 1551-B

Kramer SL, Franke KW, Huang Y-M, Baska DA (2007) Performance-based evaluation of lateral spread-ing displacement. In: Proceedings of 4th international conference on earthquake geotechnical engi-neering, paper no. 1208

Mariniello C (2007) Una procedura meccanica nella valutazione della vulnerabilità sismica degli edifici in C.A. Dissertation, University of Naples "Federico II"

Marino GG (1997) Earthquake damage inspection, evaluation and repair. Lawyers & Judges Publishing Company Inc., Tucson

Murashev A, Kirkcaldie D, Keepa C, Cubrinovski M, Orense R (2014) The development of design guidance for bridges in New Zealand for liquefaction and lateral spreading effects. NZ Transport Agency research report 553

Negulescu C, Foerster E (2010) Parametric studies and quantitative assessment of the vulnerability of a RC frame building exposed to differential settlements. Nat Hazards Earth Syst Sci. https://doi.org/10.5194/nhess-10-1781-2010

Rauch AF, Martin JR (2000) EPOLLS model for predicting average displacements on lateral spreads. J Geotech Geoenviron Eng ASCE. https://doi.org/10.1061/(ASCE)1090-0241(2000)126:4(360)

Robinson KM (2016) Liquefaction-induced lateral spreading in the 2010–2011 in the Canterbury earthquakes. NZ J Geol Geophys 55(3):1–15. https://doi.org/10.1080/00288306.2012.699895

Shamoto Y, Zhang J-M, Tokimatsu K (1998a) New charts for predicting large residual post-liquefaction ground deformation. Soil Dyn Earthq Eng 17:427–438

Shamoto Y, Zhang J-M, Tokimatsu K (1998b) Methods for evaluating residual post- liquefaction ground settlement and horizontal displacement. Soils Found 2:69–83

Shinozuka M, Feng MQ, Lee J, Naganuma T (2000) Statistical analysis of fragility curves. J Eng Mech ASCE 126(12):1224–1231

Youd TL, Perkins DM (1987) Mapping of liquefaction severity index. J Geotech Eng 113(11):1374–1392

Youd TL, Hansen CM, Bartlett SF (2002a) Revised multilinear regression equations for prediction of lateral spread displacement. J Geotech Geoenviron Eng 128:1007–1017

Youd TL, Hansen CM, Bartlett SF (2002b) Revised multilinear regression equations for prediction of lateral spread displacement. J Geotech Geoenviron Eng ASCE 128(12):1007–1017

Zhang G, Robertson PK, Brachman RWI (2004) Estimating liquefaction-induced lateral displacements using the standard penetration test or cone penetration test. J Geotech Geoenviron Eng ASCE 130(8):861–871

Affiliations

Fausto Somma[1] · Maxim Millen[2] · Emilio Bilotta[3] · Alessandro Flora[3] · Antonio Viana Da Fonseca[4]

Maxim Millen
maxim.millen@gmail.com

Emilio Bilotta
bilotta@unina.it

Alessandro Flora
flora@unina.it

Antonio Viana Da Fonseca
viana@fe.up.pt

[1] Department of Structures for Engineering and Architecture, University of Naples Federico II, Naples, Italy

[2] Department of Civil and Natural Resources, University of Canterbury, Christchurch, New Zealand

[3] Department of Civil, Architectural and Environmental Engineering, University of Naples Federico II, Naples, Italy

[4] CONSTRUCT-GEO, Faculty of Engineering, University of Porto, FEUP, Porto, Portugal